

# Topographically controlled, breaking-wave-induced macrovortices. Part 1. Widely separated breakwaters

By M. BROCCINI<sup>1</sup>, A. KENNEDY<sup>2</sup>, L. SOLDINI<sup>3</sup>  
AND A. MANCINELLI<sup>3</sup>

<sup>1</sup>D.I.Am., Università di Genova, 16145 Genova, Italy

<sup>2</sup>Department of Civil & Coastal Engineering, University of Florida, Gainesville,  
FL 32611-6590, USA

<sup>3</sup>Istituto di Idraulica, Università Politecnica delle Marche, 60131 Ancona, Italy

(Received 5 June 2003 and in revised form 18 November 2003)

In this and the companion paper (Part 2) we examine experimentally, computationally, and analytically the behaviour of breaking-wave-induced macrovortices during startup conditions. Widely separated breakwaters and rip current topographies are chosen as opposite ends of the parameter space. Part 1 examines generation mechanisms using phase-resolving and phase-averaged approximations, and suggests several simple predictive relations for general behaviour. Vortex trajectories and shedding periods for wave breaking on widely spaced breakwaters are also considered in detail. Results show broad agreement with theoretical trajectories. Predictions of vortex shedding periods on breakwater heads show excellent agreement with computations. Part 2 examines startup macrovortices on rip current topographies using computations and laboratory experiments, and changes in behaviour as the system transitions from wide to narrow gap width.

---

## 1. Introduction

In the nearshore ocean, variations in longshore bathymetry are ubiquitous. These may be natural, as bottom sand is rearranged in a complex feedback among waves, currents and sediment; they may be manmade, as found on jetty or breakwater heads. In all cases, these bathymetric variations modify the incident wave field. In many cases waves break on these features, with different intensity at different locations. As shown theoretically (Peregrine 1998, 1999; Bühler 2000), differential wave breaking generates vorticity which reorganizes in the form of large-scale horizontal eddies with a vertical axis, also known as macrovortices.

The only detailed numerical study of breaking-wave-generated vortices to date has focused on vortex generation on longshore-uniform topographies (Bühler & Jacobson 2001). Here, *ad hoc* offshore amplitude variations in wave height were necessary to give longshore variability in breaking and thus generate vortices. However, longshore variation in bottom elevation is the theoretically most sound source of stationary long-term longshore variations in wave height. Numerical studies of topographically controlled rip currents have predicted vortex shedding on bar edges (e.g. Chen *et al.* 1999; Yu & Slinn 2003) with vortices advected offshore. Numerical studies of wave breaking on single breakwaters (Broccini *et al.* 2002) have shown similar vortex generation, but with vortices advected towards the shoreline.

Field observations of nearshore vortices are rare. Smith & Largier (1995) observed, using acoustic techniques, rip current vortices with radii  $R$  of order 10s of m, but did not investigate their source. To our knowledge there are no reported laboratory observations specifically focused on breaking-wave-generated macrovortices, in part because they are difficult to measure using fixed current meters.

The generation and transport of startup macrovortices for topographically controlled wave breaking forms the subject of this paper and its companion, Part 2 (Kennedy *et al.* 2004). Two typical situations are to be examined in detail: wave breaking at breakwater heads and on rip current topographies. Each represents an extreme of the problem parameter space. Vortices generated on opposite ends of a breakwater are widely separated, typically have little mutual interaction and travel towards the shoreline mainly because of the wave field and self-advection. The latter represents the contribution to the vortex motion due to the presence of a sloping bed which forces the vortex to move along isobaths. The intensity of the self-advection of a large-scale vortex on a beach can be modelled by regarding the macrovortex as a portion of a vortex ring with radius equal to the distance between the macrovortex and the shoreline (e.g. Bühler & Jacobson 2001). In contrast, oppositely signed vortices in a rip current topography are extremely close together, have significant interactions, and may travel offshore as a pair. In this case the vortex pair made of two vortices of approximately equal strength ( $\Gamma$ ) but opposite sign and with separation  $a$  move under the action of mutual interaction at a speed of about  $\Gamma/(2\pi a)$ . The problem is highly complex as many processes of similar strength operate simultaneously.

Vortex shedding at the lee-side of a topographic obstacle is a well-documented phenomenon and various results are available to characterize the main features of the instability of the wake both in marine (e.g. Lloyd & Stansby 1997) and atmospheric environments (e.g. Schär & Smith 1993*b*; Schär & Durran 1997). Once transition to vortex shedding occurs a number of parameters like the vortex size and the shedding period are analysed as useful for both hindcasting and forecasting purposes (e.g. Schär & Smith 1993*b*). However, most of those studies have used simple approaches in which a steady current meets the obstacle over a flat bottom. Only very recently have attempts been made to quantify the wake instability caused by an oscillatory shallow-water flow around an island (Lloyd, Stansby & Chen 2001). We here aim to evaluate the properties of startup macrovortices in more realistic nearshore flow configurations in which breaking waves interact with topographic features like longshore bars or submerged breakwaters over a uniformly sloping beach.

In the first portion of this paper (§2), we define the problem and introduce scaling arguments; next we examine and tie together several different approaches to looking at the generation of vorticity and circulation on longshore-varying topographies. In §3, we examine startup vortices on breakwater heads with numerical solutions of the nonlinear shallow-water equations (NSWE). The focus here is mainly on determining characteristics of startup vortices like the shedding period and the vortex trajectory. Section 4 summarizes results and concludes the paper.

The companion paper (Kennedy *et al.* 2004) examines vortex generation and transport on rip current topographies, and bridges the two extremes represented by single breakwaters and rip current configurations.

## 2. Theoretical development and scaling

Here, we analyse vorticity and circulation arising from wave dissipation using three different approaches. In the bore evolution approach, the amount of vorticity

or circulation generated by the bore is directly related to the depth jump across a bore and no modelling is required other than suitably following the breaker. This is naturally embodied in the wave-resolving NSWE. Other wave-resolving approaches can be used, like Boussinesq-type models, in which the energy dissipation process and the induced circulation are accounted for by a parametric formulation which models the dynamics occurring at the breaker's front. A third approach stems from scale-separating fluid motion into short waves and currents, and then averaging over the short timescale. In the following, we examine the circulation arising in various representations of dissipating waves, and show how they interrelate.

### 2.1. Bore dissipation models

The two greatest advantages of studies based on the wave-resolving NSWE approach are that they have some fundamental validity for finite wave heights, and that dissipation follows directly from the bore geometry. This was exploited by Peregrine (1998, 1999), who showed that the instantaneous rate of change of circulation around a closed material curve passing once only through a single bore is equal to the rate of energy loss through that bore:

$$\frac{D\Gamma}{Dt} = E_D \tag{2.1}$$

where

$$\Gamma \equiv \oint \mathbf{U} \cdot d\mathbf{l} \quad \text{and} \quad E_D \equiv \oint \mathbf{D} \cdot d\mathbf{l} = \frac{g(d_1 - d_2)^3}{4d_1d_2} \tag{2.2}$$

and  $d_1$  and  $d_2$  are the first and second water levels encountered by the curve on either side of the bore while  $\mathbf{U} = (U, V)$  and  $\mathbf{D} = (D_x, D_y)$  are respectively the depth-averaged velocity and the dissipative body force caused by turbulent bores.

If we approximate the instantaneous bore height as  $H_B = d_1 - d_2$  and the mean water level (which may differ from the still water level) as  $d = (d_1 + d_2)/2$ , this may be rewritten as

$$\frac{D\Gamma}{Dt} = \frac{gH_B^3}{4d^2 - H_B^2} \tag{2.3}$$

where, again, we consider the instantaneous wave height and water depth at the bore. Care must be taken here to ensure that the sense of the curve is consistent: if the material curve encounters the crest first and then the trough the wave height is positive, but is negative if the curve first encounters the trough.

### 2.2. Phase-resolving models with parametric breaking

The best examples of phase-resolving models without bore dissipation built into the numerical discretization are the various types of wave breaking schemes for Boussinesq wave models (Brocchini, Drago & Iovenitti 1992; Schäffer, Madsen & Deigaard 1993; Chen *et al.* 1999; Kennedy *et al.* 2000; Veeramony & Svendsen 2000; and numerous others). These schemes differ considerably from each other but generally have two commonalities, which tend to give them similar performance: dissipation is localized on the front face of the breaking wave and dissipative forces are momentum-conserving.

Localizing breaking forces on the front face of waves mimics bore dissipation, as bores do not form naturally in these nonlinear-dispersive models. Momentum-conserving breaking is essential for the proper representation of breaking-wave-induced processes such as setup – without it, all predictions are completely wrong. (Veeramony & Svendsen (2000) also include a term arising from breaking-induced

differences in bottom pressure that is proportional to bottom slope. Other representations neglect this as being small compared to other processes.)

A typical representation is

$$\mathbf{u}_{\alpha,t} + (\mathbf{u}_{\alpha} \cdot \nabla) \mathbf{u}_{\alpha} + g \nabla \eta + \text{many other terms} = \mathbf{D} \quad (2.4)$$

where  $(\cdot)_{,t}$  represents partial differentiation with respect to  $t$  and  $\mathbf{u}_{\alpha}$  is a specific characteristic Boussinesq velocity (there are innumerable definitions for characteristic Boussinesq velocities). Note that the dissipative breaking force must be defined as  $\mathbf{D} \equiv (\nabla \cdot \mathbf{F})/d$ , where  $\mathbf{F}$  is a symmetric two-dimensional tensor. As noted by both Bühler (2000) and Kennedy *et al.* (2000), division by the total water depth  $d = h + \eta$  ( $h$  being the still water level and  $\eta$  the water surface displacement) is necessary in such representations for a momentum-conserving process.

Generation of circulation then arises naturally: ignoring bottom friction terms etc. gives

$$\frac{D\Gamma}{Dt} = \oint \mathbf{D} \cdot d\mathbf{l} + O(\mu^2) \quad (2.5)$$

where  $O(\mu^2)$  represents contributions from dispersive Boussinesq terms. It is not in general possible to make statements about rotational dispersive flow in Boussinesq models as significant deficiencies are found in many derivations (see Gobbi, Kirby & Kennedy 2000). This leads to the result that leading-order rotational motion in Boussinesq-type equations follows discussions in Bühler & Jacobson (2001) very closely.

### 2.3. Phase-averaged models

Neglecting bottom slope effects, surface shear stresses, and variations in atmospheric pressure, it may be shown, after Mei (1983), that

$$\frac{\partial \tilde{U}}{\partial t} + \tilde{U} \cdot \nabla \tilde{U} = -g \nabla \bar{\eta} - \frac{\nabla \cdot (\mathbf{S} + \mathbf{S}')}{\bar{d}} - \frac{\tau}{\bar{d}} \quad (2.6)$$

where  $\bar{d} = h + \bar{\eta}$  is the phase-averaged total water depth,  $\tilde{U}$  is the mass-transport velocity, defined as  $\tilde{U} \equiv \mathbf{U} + \mathbf{M}/\bar{d}$ ,  $\mathbf{M}$  being the wave-induced volume transport, and  $\tau$  is the bottom frictional stress. All definitions of stresses and energies here neglect densities, as these are unimportant in discussions of circulation for constant-density fluids. Radiation stresses here are divided into organized wave-induced stresses  $\mathbf{S}$  and contributions from turbulent fluctuations  $\mathbf{S}'$ . Typically these turbulent stresses are ignored, since they are important only in the surf zone, and this is exactly the region where commonly used small-amplitude radiation stress approximations show considerable error. The overall error then includes contributions from both terms in uncertain proportion.

Phase-averaged equations for wave evolution vary considerably. To a reasonable level of approximation, wave action relations based on geometrical optics show many relevant features. Consistent with the purposes of this paper, and for simplification, we look at the initial stages of vorticity generation, when mean currents and departures from still water levels are small. In some ways this resembles the analysis of Bühler & Jacobson (2001), in which a Reynolds-type decomposition of the flow was used to separate wave and current components, and in which seabed friction effects were neglected. However, we here allow for frequency dispersion which gives our analysis a somewhat broader area of application. This also builds on previous analyses by Longuet-Higgins (1973) and Dingemans, Radder & De Vriend (1987)

who examined the relationship of breaking dissipation to mean current forcing, but did not specifically examine generation of circulation although it would have been straightforward in either case.

In summary, equation (2.6) can be simplified by neglecting the nonlinear advective term because of the ‘small current approximation’, by neglecting the turbulence-induced stresses with respect to the wave-induced ones, by neglecting the bed friction as important only over long time spans (Bühler & Jacobson, 2001) and by approximating  $\bar{d}$  with  $h$ . This is added to the other four relations available for the problem, i.e. to the wave energy flux equation, the linear dispersion relationship, the ray-tracing equation (to examine varying depth), and the definitions for the radiation stresses. In detail the five sets of equations to be solved are

$$E_{,t} + \nabla \cdot (E \mathbf{C}_g) = -DhC_g, \quad (2.7)$$

$$\tilde{U}_{,t} + g\nabla\bar{\eta} = -\frac{1}{h}\nabla \cdot \mathbf{S}, \quad (2.8)$$

$$\omega^2 = gk \tanh kh, \quad (2.9)$$

$$\cos\theta\theta_{,x} + \sin\theta\theta_{,y} - \sin\theta\frac{C_{,x}}{C} + \cos\theta\frac{C_{,y}}{C} = 0, \quad (2.10)$$

$$S_{xx} = En \cos^2\theta + E\left(n - \frac{1}{2}\right), \quad S_{xy} = En \sin\theta \cos\theta, \quad S_{yy} = En \sin^2\theta + E\left(n - \frac{1}{2}\right), \quad (2.11)$$

$$n = \frac{1}{2} \left( 1 + \frac{2kh}{\sinh 2kh} \right), \quad (2.12)$$

where  $E \equiv gH^2/8$  is the kinematic wave energy per unit surface area,  $D$  is the breaking pseudo-force per unit volume (acting in the opposite direction to the group velocity),  $\theta$  is the wave angle relative to the  $x$ -coordinate,  $C = \omega/k$  is the wave phase speed,  $C_g = nC$  is the group velocity, and  $\mathbf{C}_g = C_g(\cos\theta, \sin\theta)$ .

Considering only the  $x$ -momentum for simplicity, and substituting definitions for radiation stresses directly into (2.8) we obtain

$$\begin{aligned} \tilde{U}_{,t} = & -\frac{1}{h} [\cos\theta([En \cos\theta]_{,x} + [En \sin\theta]_{,y}) - En \sin\theta(\cos\theta\theta_{,x} + \sin\theta\theta_{,y}) \\ & + [E(n - 1/2)]_{,xx} - g\bar{\eta}_{,x}. \end{aligned} \quad (2.13)$$

The first set of terms on the right-hand side can be used to introduce the dissipation directly using (2.7)

$$\begin{aligned} \tilde{U}_{,t} = & -\frac{1}{h} \left[ \cos\theta \left( -\frac{E_{,t}}{C} - Dhn - En \cos\theta \frac{C_{,x}}{C} - En \sin\theta \frac{C_{,y}}{C} \right) \right. \\ & \left. - En \sin\theta(\cos\theta\theta_{,x} + \sin\theta\theta_{,y}) + [E(n - 1/2)]_{,xx} - g\bar{\eta}_{,x}. \right] \end{aligned} \quad (2.14)$$

Collecting terms, using trigonometric identities and reverting back to two horizontal dimensions:

$$\tilde{U}_{,t} = Dn + \frac{\mathbf{E}_{,t}}{Ch} - g\nabla\bar{\eta} - \nabla \left[ \frac{E(n - 1/2)}{h} \right] \quad (2.15)$$

where  $\mathbf{D} \equiv (D_x, D_y) = D(\cos\theta, \sin\theta)$ , and similarly  $\mathbf{E} \equiv E(\cos\theta, \sin\theta)$ .

As the mass transport velocity is appropriate for examining rates of circulation change, we take a line integral and arrive at

$$\Gamma_{,t} = \oint \left( \frac{\mathbf{M}_{,t}}{h} + n\mathbf{D} \right) \cdot d\mathbf{l}. \quad (2.16)$$

The second term related to wave breaking dominates in most cases. Thus the generation of circulation is directly related to the wave-breaking pseudo-force per unit volume, as might be expected. A comparison of (2.3), (2.5) and (2.16) shows almost identical formulations, with dispersive effects in the scale-separated formulation as the only difference.

To our best estimation, the  $\mathbf{M}_{,t}/h$  term exists in non-conservative form because the wave evolution equations used do not include diffraction, which would modify energy transport and radiation stresses (see also Dingemans *et al.* 1987). Clearly, from Kelvin's circulation theorem, circulation cannot be generated in the absence of wave breaking. As a side note, if the Eulerian velocity  $\mathbf{U}$  were used in (2.16) instead of the mass transport velocity  $\tilde{\mathbf{U}}$ , the offending term would disappear. However, as the mass-transport velocity is the time-averaged velocity of a water column in shallow water, it is the proper choice. For the strong current case, it would be straightforward to include advective terms in the forced shallow-water equations: combined with a conservation of mass equation, and following the usual steps in examining circulation, the partial derivative  $\Gamma_{,t}$  in (2.16) would change to the material derivative  $D\Gamma/Dt$ . However, as the wave evolution equations do not include the effects of wave-current interaction, this would not be consistent. In any case, we do expect that the rate of change of circulation of a material curve should also depend on the dissipation strength  $\mathbf{D}$  as given in (2.16), since no circulation can be generated in the absence of breaking.

### 2.3.1. Relationship between setup and circulation

As irrotational forcing, wave-induced setup cannot generate steady circulation. However, both setup and circulation are generated by breaking-wave forces. Because of this, setup may be used to estimate generation of circulation across a breaking event in the somewhat restrictive situation of small velocities at the ends of the path considered.

To do this, we integrate along the wave ray from point '1', offshore of the breaking event, i.e. of coordinate  $x_1$ , to point '2', which is onshore, i.e. of coordinate  $x_2$ . Assuming quasi-steady breaking and using equation (2.15) we find

$$\left. \begin{aligned} \int_{x_1}^{x_2} n \mathbf{D} dx &= g (\eta_2 - \eta_1) + \left( \frac{E(n-1/2)}{h} \right)_2 - \left( \frac{E(n-1/2)}{h} \right)_1 \\ (\Gamma_{,t})_{12} &= g (\eta_2 - \eta_1) - g (\eta_{sd2} - \eta_{sd1}), \end{aligned} \right\} \quad (2.17)$$

where  $\eta_{sd1}$  and  $\eta_{sd2}$  are the steady-wave setdowns at each location (e.g. Dean & Dalrymple 1984). Thus, the rate of generation of circulation associated with a wave-breaking event is directly linked to the change in mean water surface elevation across that breaking event, with corrections for the irrotational pressure setdown associated with the waves. Summation of all corrected surface elevation jumps in the closed circuit gives the total rate of generation of circulation. As with Peregrine (1998), the correct sense of the summation must be preserved: jumps in the direction of wave travel are positive, while those opposite to the wave direction are negative.

### 2.3.2. Estimates of phase-averaged circulation change

The phase-averaged approximation suffers from the disadvantage that breaking dissipation is arbitrary in the derivation. Here, we make some simple approximations to estimate circulation change at startup for waves breaking on a bar or breakwater with crest height  $h_c$ , but not in an adjacent deeper channel. The differential breaking

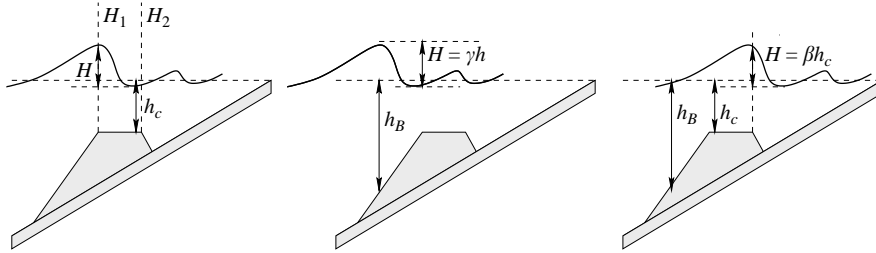


FIGURE 1. Sketch of three types of wave breaking at a bar-like topographic obstacle.

caused by this non-uniform topography thus generates circulation. All breaking waves are assumed to be in shallow water and all waves are assumed to be shore-normal. We further use the rigid-lid assumption of small departures from the still water level, and quasi-steady breaking waves so that the unsteady wave contribution in (2.16) vanishes. These estimates may prove useful for many different applications.

Three different breaking assumptions are to be used. These are (see figure 1):

(a) waves break only on the bar crest at depth  $h_c$  and finish with height  $H = \beta h_c$  (steep-fronted wide reef);

(b) waves break on the slope according to the depth-limited criterion  $H = \gamma h$ ,  $h \leq h_B$  in which  $h_B$  gives the depth at which breaking first occurs (gentle slope, narrow crest);

(c) waves break on the slope according to the depth-limited criterion  $H = \gamma h$ , and continue breaking on the bar crest, finishing with height  $H = \beta h_c$  (gentle slope, wide crest). Breaking types (a) and (b) are probably bracketing estimates, as waves are unlikely to break only on the bar crest as assumed in type (a), but are also unlikely to stop breaking as soon as the local slope becomes flat, as assumed in type (b). Type (a) always leads to a greater circulation for the same incident waves, as breaking is in shallower water. Type (c) is a combination of types (a) and (b), and may be the most physically plausible scenario in many situations.

For breaking type (a), the constant water depth on the bar crest simplifies things considerably and (2.16) may be integrated analytically to arrive at

$$\Gamma_{,t} = \oint \mathbf{D} \cdot d\mathbf{l} = \frac{1}{h_c} (E_1 - E_2) \quad (2.18)$$

where  $E_1$  and  $E_2$  are the energies at the seaward and shoreward ends of the bar crest, computed without density. Since energy is proportional to the square of the wave height in the leading-order formulation, the rate of change of circulation is proportional to the difference of the squares of the wave heights, measured just before and just after the bar (figure 1). This case is most appropriate for steep bar or breakwater fronts with a wide flat crest, or for waves breaking on coral reefs.

Assuming that the wave height at the shoreward end of the bar or breakwater crest is represented by  $H_2 = \beta h_c$ , we arrive at

$$\Gamma_{,t} = \frac{g}{8} \left[ H_0^2 \frac{C_{g0}}{g^{1/2} h_c^{3/2}} - \beta^2 h_c \right] \quad (2.19)$$

where  $H_0$  and  $C_{g0}$  are the wave height and group velocity at a given location offshore of the bar.

For breaking type (b), depth-limited breaking is assumed on the front slope of the breakwater, with cessation of breaking once the bar slope reaches zero. For

shore-normal waves breaking in shallow water, the breaking dissipation becomes

$$D_x = -\frac{5g}{16}\gamma^2 h_{,x}, \quad h \leq h_B. \quad (2.20)$$

After a change of integration variable in (2.16) from  $x$  to  $h$ , the integral may be evaluated analytically to give

$$\Gamma_{,t} = \frac{5g\gamma^2}{16}(h_B - h_c). \quad (2.21)$$

Finally, the depth for shore-normal waves breaking in shallow water may be estimated as (e.g. Dean & Dalrymple 1984)

$$h_B = (H_0^2 C_{g0})^{2/5} \gamma^{-4/5} g^{-1/5} \quad (2.22)$$

or through any other appropriate method for more complex situations.

One further option (type (c)) may be considered, where the wave breaks like  $H = \gamma h$  on the slope, and continues to break on the flat top of the bar, finishing with height  $H = \beta h_c$ . The final rate of change of circulation here becomes

$$\Gamma_{,t} = \frac{5g\gamma^2}{16}(h_B - h_c) + \frac{gh_c}{8}(\gamma^2 - \beta^2). \quad (2.23)$$

Estimates of circulation here always lie in between those of types (a) and (b).

Thus, if  $E_1 \gg E_2$ , circulation increases with the square of wave height for breaking type (a), while if  $h_B \gg h_c$  in types (b) and (c), circulation increases proportionally to wave height to the four fifths power. We should emphasize again that differences between still water level and mean water level have been neglected in all cases, but due to the simplistic nature of the breaking assumptions, this hardly seems significant.

Estimates of rates of circulation generation are tested in the companion paper Part 2, and in related papers. In Kennedy (2003), these estimates are combined with a very simple dynamical model of rip currents to predict steady and unsteady properties in a rip neck, while Kennedy & Thomas (2004) relate them to overall properties in a rip current, including mean circulation and characteristic timescales.

#### 2.4. Geometrical controls on startup vortices

For general breakwater/bar geometries, the quantitative prediction of vortex strengths and trajectories becomes quite difficult: as startup vortices are found in areas with strong variations in breaking, it can be difficult to define a characteristic depth. Even characteristic background velocities can become difficult in strongly sheared regions. However, using circulation relations combined with conservation of mass, some vortex self-interaction and mutual interaction relations, relating general vortex behaviour to changing geometry becomes relatively straightforward. In some relatively simple cases, good quantitative predictions may be found.

First, consider a long string of breakwaters (bars) parallel to the coast, separated by gaps (rip channels). Each breakwater has crest length parallel to the shoreline  $L_c$ , and crest depth  $h_c$ . The shore-parallel gap between breakwaters has width  $L_r$ , and depth  $h_r$ . Here we assume that the flow on the bar crest is directly onshore, and flow in the channel directly offshore.



The velocity of a vortex then has three components: advection by the background velocity, mutual interaction with other vortices, and self-interaction on a sloping bed. For steady wave forcing we identify four stages of startup:

(i) All components of equation (2.15) are significant except surface elevation gradients, which are approximately zero. This is the very first fluid motion before setup has developed.

(ii) Irrotational components are in balance and contribute only to water level variations. Mutual interaction between vortices and self-interaction for vortices on a slope are the dominant processes.

(iii) Macrovortices leave the areas of generation and self-interaction slope effects become less important than mutual interaction.

(iv) Interaction between consecutively generated vortices becomes important, and friction and instabilities dissipate vortex strengths. This stage at least approaches the beginning of stochastically steady-state conditions.

In stage (i) conditions, the velocity of the vortex has three components: advection by the background velocity, mutual interaction with other vortices, and self-interaction on a sloping bed. Background velocities may be related to larger scale currents or to the fluid accelerations that eventually lead to wave setup; in any case they include all motions not specifically caused by the breaking-wave-induced macrovortices. Noting again that mean surface elevations immediately at startup are approximately zero and if there are no significant pre-existing larger scale currents, the general shoreward acceleration at the crest can be estimated from (2.15). Of the terms on the right-hand side, analysis of typical situations shows that the strongest by far is that related to the breaking wave dissipation, i.e.  $U_{bg,t} \approx D_x$ , whose magnitude is approximately  $E_D/L_B$ ,  $L_B$  being the size of the breaking region. Neglect of mass transport and pressure setdown terms produces some uncertainty, but uncertainties in estimating the size of the breaking region are likely to be the dominant source of error in estimating background velocities. This approximation also assumes that macrovortex cores are near the crest of the bar, where the general breaking-wave-induced accelerations are strong. In reality, they travel between the shallow crest and the deeper gap, but sound theoretical attempts to represent this have proved elusive. However, as will be seen soon, this may be less important than might be supposed.

Using standard expressions for mutual advection of oppositely signed point vortices (e.g. Bühler & Jacobson 2001), the shoreward velocity is

$$U_{ma} = \frac{\Gamma}{2\pi} \left( \frac{1}{L_c} - \frac{1}{L_t} \right). \quad (2.24)$$

Again, this is highly approximate. Depending on whether the gap width is wider than the breakwater or vice versa, this may accelerate the vortex either onshore or offshore, as indicated by Peregrine (1999). Additionally, this velocity becomes small as both breakwater lengths and gap widths become large.

Finally, self-advection over a slope gives a velocity (Bühler & Jacobson 2001)

$$U_{sa} = \frac{\Gamma s}{d} \frac{1}{4\pi} \left[ \log \left( \frac{8d}{sR} \right) - \frac{1}{4} \right] \quad (2.25)$$

where  $s$  is the slope considered,  $R$  is the radius of the vortex, and  $d$  is the mean local water depth. As the vortex is likely to span shallower water on the crest and deeper water in the gap, and topography can be strongly three-dimensional, representative choices for slope (side breakwater slope, back breakwater slope, general bed slope),

and depth become difficult. Additionally, the steep slopes often found near areas of strong differential breaking introduce further complications.

Adding these together gives the total acceleration of the vortex in terms of the dissipation,  $E_D$ ,

$$\begin{aligned} U_{v,t} &= U_{bg,t} + U_{ma,t} + U_{sa,t} \\ &= E_D \left\{ \frac{1}{L_B} + \frac{1}{2\pi} \left( \frac{1}{L_c} - \frac{1}{L_t} \right) + \frac{s}{d} \frac{1}{4\pi} \left[ \log \left( \frac{8d}{sR} \right) - \frac{1}{4} \right] \right\}. \end{aligned} \quad (2.26)$$

The first and third terms in the curly brackets always force onshore flow, while the second can either force onshore (wide gap) or offshore (narrow gap) flow. As all the terms in the curly brackets are either directly ( $s$ ,  $d$ ,  $L_t$ ,  $L_c$ ) or indirectly ( $L_B$ ,  $R$ ) dependent on geometry, *initial vortex transport is mainly governed by geometric considerations.*

This analysis is highly approximate but does show many of the relevant features. However, care must be taken in following it blindly: stage (i) of startup is only valid before setups have developed and while the vortex is close to the top of the breakwater or bar. Choosing a representative slope and water depth can also be problematic. Additionally, even in the best conditions (small side slopes, long breakwater), the rip channel width must be very small according to this analysis for offshore flow to occur:  $L_t < L_B/2\pi$ . Thus the gap width must be much smaller than the breaking-width-related lengthscale, which seems unlikely.

In stage (ii) of startup, irrotational transients arising from the beginnings of setup have died down, but generation of circulation continues. The direction of travel then becomes determined by the ratio of self-advection on the slope and mutual advection by oppositely signed vortices. It thus becomes much easier for vortices to travel offshore in rip current topographies. This is a dynamically pleasing approach as the uncertainty in estimating  $U_{bg,t}$  then becomes much less important, since after irrotational startup transients die down, mass transport is a consequence of vorticity dynamics, which is mainly a function of breaking waves. Furthermore, even if macrovortices coexist with irrotational long waves, the net transport of a fluid particle by the long waves over one wave cycle is generally small when compared to the vortex motions for the cases considered.

However, even this does not tell the full story – when startup transients have become negligible, analysis may still indicate that the direction of vortex travel in rip current topographies is onshore, mainly from self-advection on the sloping bar sides, while observation shows them going offshore. This is because the side slopes of the breakwaters or bars are very limited in size. Once vortices are accelerated and self-advected into deeper water, the side slope becomes much less effective in self-advecting the vortices. In this stage (iii), mutual advection dominates for narrowly spaced periodic topographies. Such an assumption was used by Kennedy (2003) in a simplified model of a rip current neck, and was found to account for much of the observed velocity variations at startup and at other times. Companion paper Part 2 also addresses in large part phenomena during stage (iii) of startup.

Processes become much more complex during stage (iv). Interactions between consecutively generated vortices can modify strongly mutual interactions, and bottom friction begins to limit growth. As this stage continues, simple estimates of processes become more difficult. Finally, as dissipation of circulation begins to balance generation of circulation, stage (iv) gradually leads to stochastically steady-state conditions.

### 3. Startup vortices on a breakwater head

As already mentioned in these conditions macrovortices evolve under the action of the wave field and of self-advection. The latter is particularly intense for steep beach conditions. We are primarily interested in giving a characterization of some macrovortex properties like the detachment period, the size of the vortices and their typical trajectory. This has been performed by means of numerical experiments.

#### 3.1. Numerical setup

A shock-capturing, finite-volume model was used to solve the NSWE written in conservation form (see Brocchini *et al.* 2001):

$$\left. \begin{aligned} d_{,t} + (Ud)_{,x} + (Vd)_{,y} &= 0, \\ (Ud)_{,t} + \left( U^2d + g\frac{d^2}{2} \right)_{,x} + (UVd)_{,y} &= gdh_{,x} - dD_x - c_f U|U|, \\ (Vd)_{,t} + (UVd)_{,x} + \left( V^2h + g\frac{d^2}{2} \right)_{,y} &= gdh_{,y} - dD_y - c_f V|U|, \end{aligned} \right\} \quad (3.1)$$

in which  $\mathbf{D}$  is non-zero only in the presence of bores and  $c_f$  is a coefficient measuring the seabed friction expressed by a Chezy-type contribution.

The model accounts for energy dissipation at shocks ( $E_D$  of equation (2.1)), equivalent to that occurring at a hydraulic jump, through the well-known Rankine–Hugoniot conditions. The crossflow gradient of  $E_D$  determines the rate of vorticity generation at bores (e.g. Pratt 1983; Peregrine 1998). Note that it can be demonstrated that such vorticity flux is independent of the formulation of the dissipation  $\mathbf{D}$ . In other words the flux of vorticity is the same if  $\mathbf{D}$  is modelled either through jump conditions in a pseudo-inviscid framework or by means of a specific, explicit viscous formulation (Schär & Smith 1993a).

The numerical solver is based on the second-order-accurate WAF method (e.g. Toro 2001) where intercell fluxes are evaluated by means of an exact Riemann solver which allows, at a limited computational cost, a very accurate description of the solution. A flux limiter is, finally, employed to obtain non-oscillatory solutions at steep gradients. For more details on the implementation of the solver we refer the reader to Brocchini *et al.* (2001).

Being particularly suited to represent jump conditions, the shock-capturing solver models well the generation of vorticity at depth jumps and the evolution of spatially well-confined structures like macrovortices (see Brocchini *et al.* 2002).

We use a numerical domain which closely represents real-life topographic conditions in which coastal defences are placed or sand bars evolve (figure 2), and to assess the role of the beach slope  $s$  two configurations were used such that  $s = 1:10$  and  $s = 1:30$ . A radiating boundary condition has been enforced at the seaward boundary of the domain (left end in figure 2) while open conditions have been used at the lateral boundaries. All test waves as generated were sinusoidal with periods  $T_{in} = 5, 10$  s and five different wave heights  $H_{in} = 0.5, 1.0, 1.5, 2.0, 2.5$  m. The bottom friction was accounted for by varying  $c_f$  over two values only  $c_f = 0, 0.01$ .

Preliminary computations have been run to assess an optimal mesh size. This is empirically defined as the mesh which provides:

- (i) an adequate resolution of the flow features of interest, i.e. of the macrovortices;
- (ii) a reduced amount of numerical diffusion. Numerical diffusion is due to the local reduction to first-order accuracy of the scheme near steep fronts. Here the

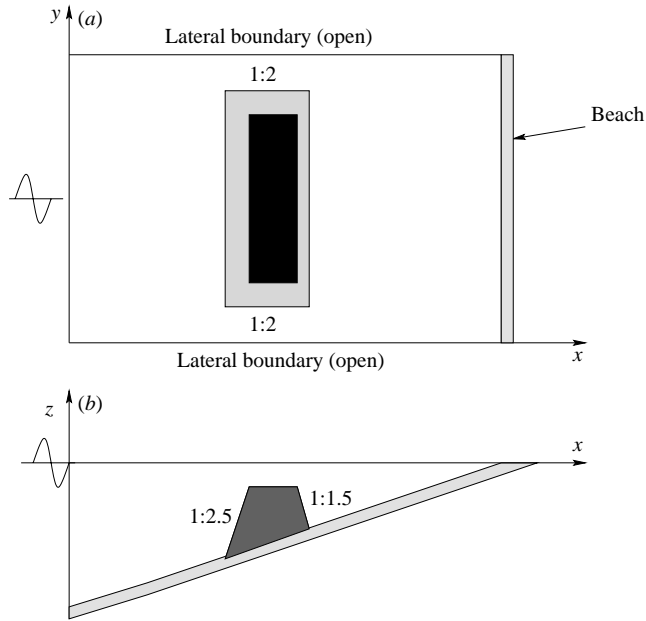


FIGURE 2. Sketch of domain used in the numerical tests for the case of a single breakwater: (a) top view, (b) side view.

leading-order truncation error is of the form

$$\nu_N \nabla^2 U \quad \text{in which} \quad \nu_N = \frac{1}{2}(1 - C)\lambda \Delta x \quad (3.2)$$

is the numerical viscosity which gives a measure of the numerical diffusion. This is proportional to the mesh size  $\Delta x$ , the celerity  $\lambda$  of the propagating signal and the Courant number  $C$ ;

(iii) numerically cheap computations.

A rectangular mesh with size  $(\Delta x, \Delta y) = (1, 2)$  m has therefore been chosen.

### 3.2. Computational results

We here focus our attention on the analysis of the main features of the flow evolution of macrovortices at startup. Vortex trajectories and detachment period of vortices have been analysed with respect to the various wave-geometry parameters. One first important result is that, confirming the intuition of Bühler & Jacobson (2001), the bed friction does not influence at all the results at hand. Also the input wave steepness weakly influences the shedding period of the vortices, which is much more strongly linked to the vortex, radius and to the lateral slope of the breakwater  $s_l$ .

#### 3.2.1. The flow evolution and the vortex trajectories

The description of the trajectory traced by the vortices in their motion towards the shoreline is of both scientific and practical interest. On one hand the trajectory can be used as a benchmark for comparing any analytical models aimed at representing the vortex motion. The practical relevance of predicting vortex trajectories resides in the possible estimate of the extent of the area over which vortices can transport passive tracers like sediments or pollutants. In other words it is, in principle, possible to give a measure of the area of influence of the vortices for any given topography and sea-state.

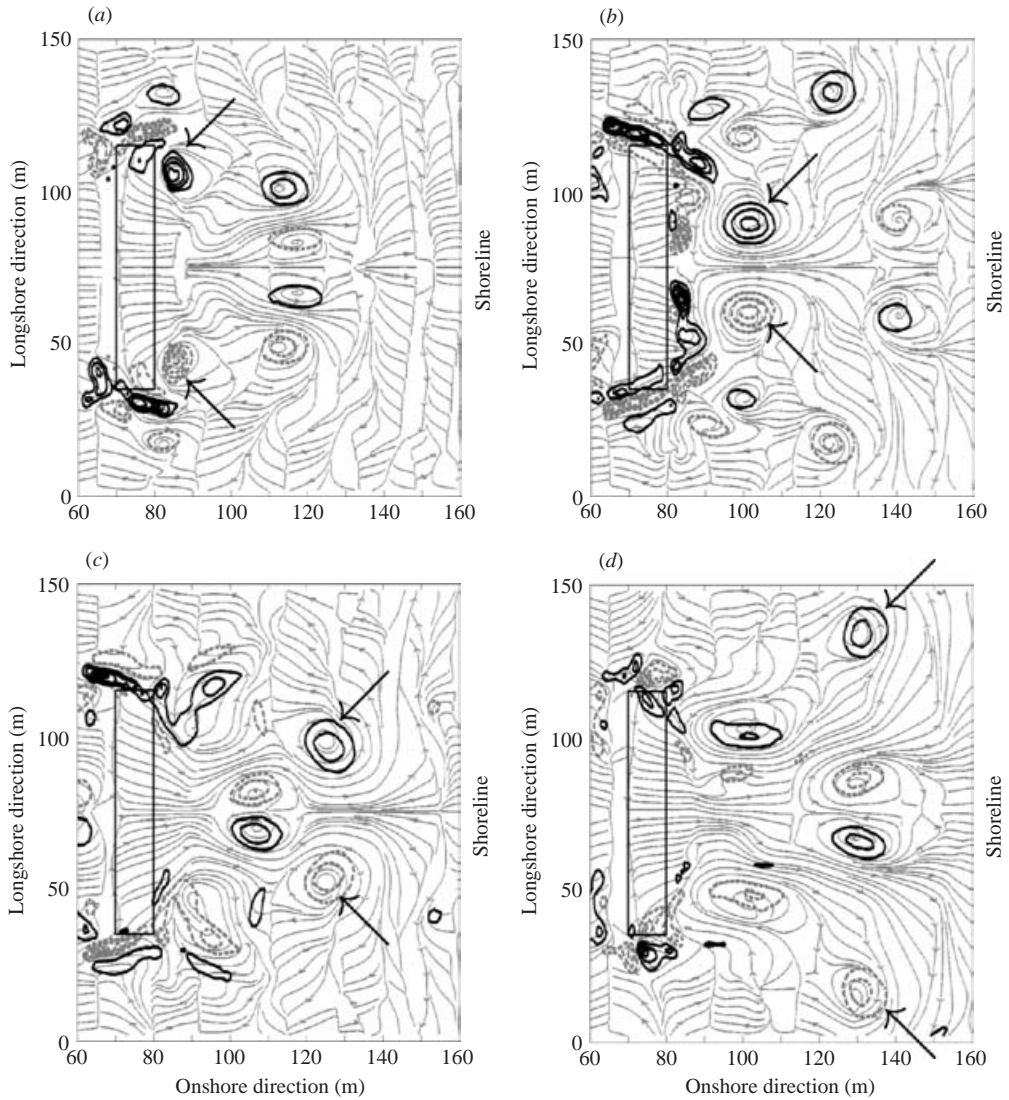


FIGURE 3. Flow patterns and shoreward macrovortices migrations for flow conditions of  $s = 1:30$ ,  $T_{in} = 5$  s,  $H_{in} = 0.5$  m and  $c_f = 0$ . The contour plots of the vorticity field are superposed on the instantaneous streamlines for times (a)  $t = 45$  s, (b) 130 s, (c) 195 s, (d) 250 s. Vorticity contour lines are solid for positive (counterclockwise) vorticity and dashed for negative (clockwise) vorticity with contour interval of  $0.2 \text{ s}^{-1}$ .

In figures 3 and 4 we illustrate the evolution of the flow due to waves which, breaking over the breakwater, generate macrovortices which subsequently propagate towards the shore over beaches of different slopes (figure 3  $s = 1:30$ , figure 4  $s = 1:10$ ). These two examples characterize well the flow evolution of all the other cases and, hence, are taken as representative of the different vortex motion over a 1:30 and a 1:10 beach. The streamlines quite clearly show the motion of the macrovortices towards the shoreline. For clarity, contour lines of the vorticity field defined through the single vorticity component  $\omega = V_{,x} - U_{,y}$  have been superposed to better identify the cores of the vortices. Arrows have also been used to locate a given pair of vortices which,

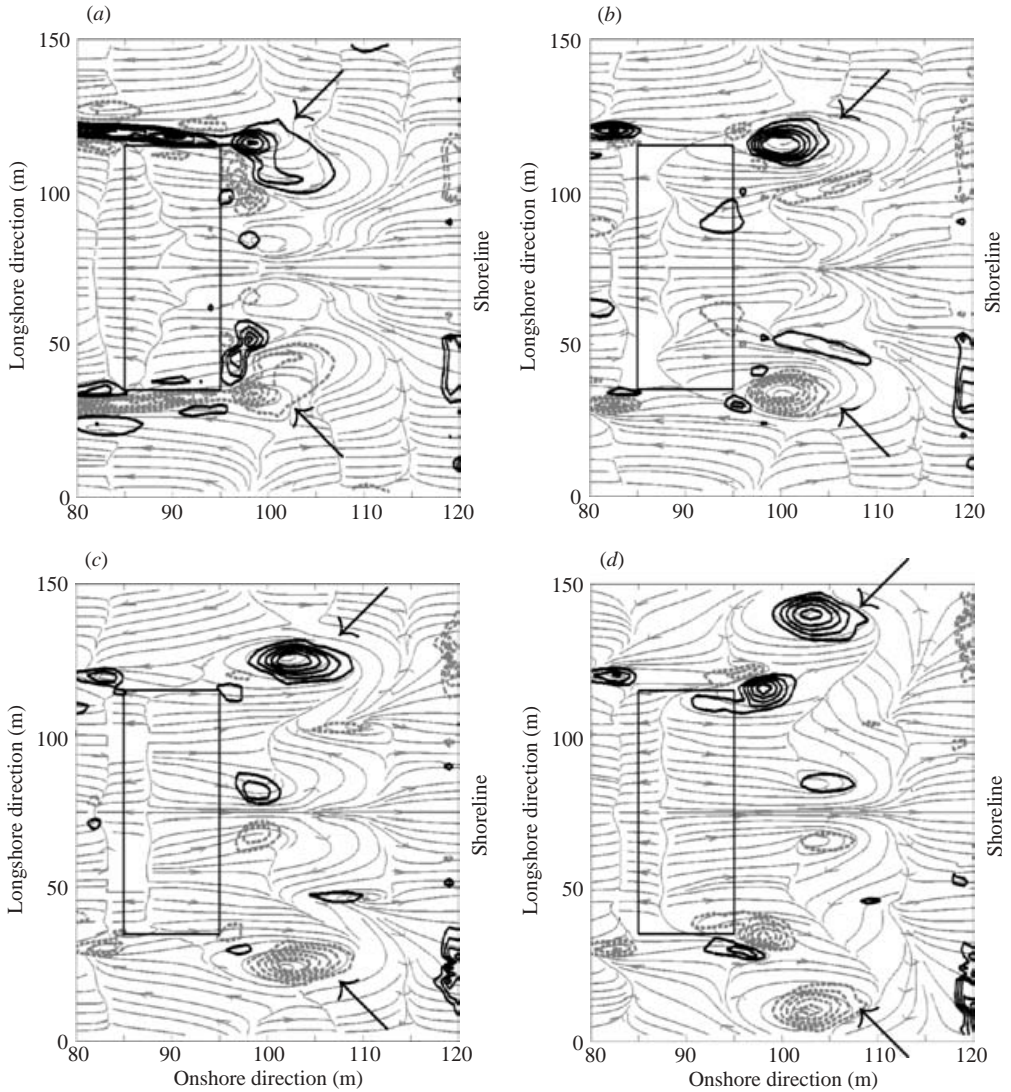


FIGURE 4. Flow patterns and shoreward macrovortex migrations for flow conditions of  $s = 1:10$ ,  $T_{in} = 5$  s,  $H_{in} = 0.5$  m and  $c_f = 0$ . Snapshots are for times (a)  $t = 5$  s, (b) 25 s, (c) 45 s, (d) 65 s. For other details see caption of figure 3.

shed at the breakwater, move towards the shore along tracks which are reproduced in detail on figure 5.

We can see that for the milder slope conditions macrovortices move along a rather complex route. In the following description the generation instant is taken as the zero time datum. The majority of the early motion ( $t < 60$  s) is of stage (ii) type where vortices, due to the strong interaction with the steep slopes of the breakwater, self-adveat around the corner from the side slope, and propagate parallel to the breakwater itself (figure 3a). Once the vortices meet along the centreline of the breakwater, they mutually adveat towards the shoreline under stage (iii) conditions. Until  $t \approx 190$  s, the route is almost shore normal and almost coincides with the breakwater mid-line (figure 3b, c). This shoreward migration is due to coupling with the opposite-signed

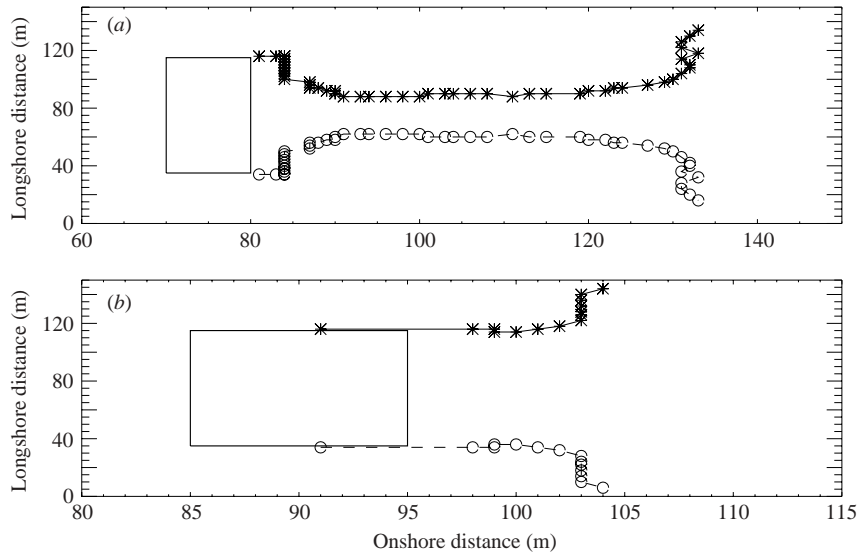


FIGURE 5. Typical cases of macrovortex trajectories for different beach slopes. The thicker black line represents the breakwater berm, while trajectories of positive vortices are given in continuous lines and those of negative vortices in dotted lines. (a) Trajectories of vortices emitted for flow conditions of  $s = 1:30$ ,  $T_{in} = 0.5$  s,  $H_{in} = 0.5$  m,  $c_f = 0$ , shoreline at  $x = 150$  m. (b) Trajectories of vortices emitted for flow conditions of  $s = 1:10$ ,  $T_{in} = 0.5$  s,  $H_{in} = 0.5$  m,  $c_f = 0$ , shoreline at  $x = 115$  m.

vortex shed from the opposite edge of the breakwater, hence forming a vortex pair. Nearer the shoreline, the pair splits and for the last 50 s of motion vortices move diagonally, i.e. still towards the shore but away from the breakwater midline (figure 3*d*), the separation distance from the midline increasing with the flow intensity. This shoreline motion is qualitatively similar to experiments reported by Centurioni (2002), and readers should consult this reference for a detailed experimental investigation of vortex couples near shorelines.

Complicating matters are oppositely signed vortices generated both at the shoreline and at the breakwater during the previous/later wave cycles. They do not appear to have a large initial influence on the bar-generated macrovortices as they travel to the shoreline. However, by the end of the simulation, stage (iv) conditions are obvious, where interactions between consecutively generated vortices are important. In particular the oppositely signed pair generated at the breakwater (figure 3*b*) and located slightly seaward of the pair under analysis (figure 3*c*) moderately interacts with it, being advected towards the shoreline.

For the steep slope (figure 4) macrovortices are shed from the breakwater side slope but their route to the shore is less complex. After reorganization, vortices migrate along a diagonal track which bends away from the breakwater. The overall effect of the steep breakwater slopes which controlled vortex movement for the gentler 1:30 beach slope appears much reduced. Here, breakwater-generated vortices seem to interact more strongly with the shore vortices generated at around  $x = 120$  m which are a factor 3 closer to the shore and stage (iii) behaviour begins much sooner. Mutual advection with these shore vortices tends to move macrovortices away from the breakwater centreline and into the gap, as observed. During the later stages, consecutively generated vortices again become important.

In figure 5 we summarize the information on the vortex trajectories for the two cases illustrated in figures 3 and 4. With similar graphs it is quite easy to analyse many important features of macrovortex evolution.

To summarize, for both the steep and gentle slopes, vorticity patches are generated, strengthened, and reorganized into coherent vortices which are transported shoreward by the background flow acceleration and self-advection along the sloping breakwater sides. The major difference occurs once vortices reach the shoreward edge of the breakwater. For the gentle slope, stage (ii) self-interaction remains the strongest process and vortices continue migrating along the shoreward end of the breakwater, while for the steep slope, mutual interaction with closer shore vortices (or possibly self-interaction of the breakwater vortices with the shoreline) appears stronger and stage (iii) mutual-interaction-dominated conditions begin much earlier. In both simulations, the situation becomes progressively more complex as vortices continue to be generated.

### 3.2.2. Detachment period

For widely spaced breakwaters, we examine the detachment period  $T_d$  of the first vortex, which appears early enough that stage (i) conditions represent a good approximation for most cases. We can give a theoretical estimate for  $T_d$  using simple dimensional arguments. We define  $T_d$  as the time taken for a vortex to reach, under the action of the breaking waves and of self-advection, a distance from the breakwater equal to its own size  $R$ . Then if we designate by  $A_d$  the onshore acceleration at which the vortex speeds away from the breakwater we have

$$R \approx \frac{A_d T_d^2}{2} \implies T_d \approx \sqrt{\frac{2R}{A_d}}. \quad (3.3)$$

Equation (2.26) may then be used to compute the vortex onshore acceleration and thus the detachment period. For the special case of widely separated breakwaters, significant simplifications are possible. To begin, the mutual interaction term (middle term in the curly brackets in (2.6)) is small and is eliminated (numerical experiments show it influences by less than 1% the estimated value of  $T_d$ ). Numerical and experimental evidence shows that  $L_B \approx 2R$  so we introduce this. Then taking the reference local depth as the computed mean depth at detachment,  $d_d$ , we obtain the following estimate:

$$T_d \approx \sqrt{\frac{2R}{E_D} \left\{ \frac{1}{\frac{1}{2R} + \frac{s_l}{d} \frac{1}{4\pi} \left[ \log \left( \frac{8d}{s_l R} \right) - \frac{1}{4} \right]} \right\}} \quad (3.4)$$

in which  $s_l$  is the side slope of the breakwater, here  $s_l = 1:2$ , accounting for the self-advection in the onshore direction. The dependence on the local breaking intensity is measured through  $E_D$  which is computed with (2.3).

Note that according to (3.4)  $T_d$  is evaluated on the basis of local flow properties rather than on global properties as with other available descriptions (e.g. Schär & Smith 1993*b*). This is obviously due to the much more complicated flow investigated here in comparison to that evaluated in the available literature.

A comparison between estimated detachment period,  $T_d$ , evaluated using (2.3), and (3.4), and results from the numerical simulations is given in figure 6. It is clear that the dimensionless evaluated detachment period  $T_d^e / (\sqrt{h_c/g})$  of equation (3.4), reported along the ordinate, slightly overestimates the dimensionless measured value



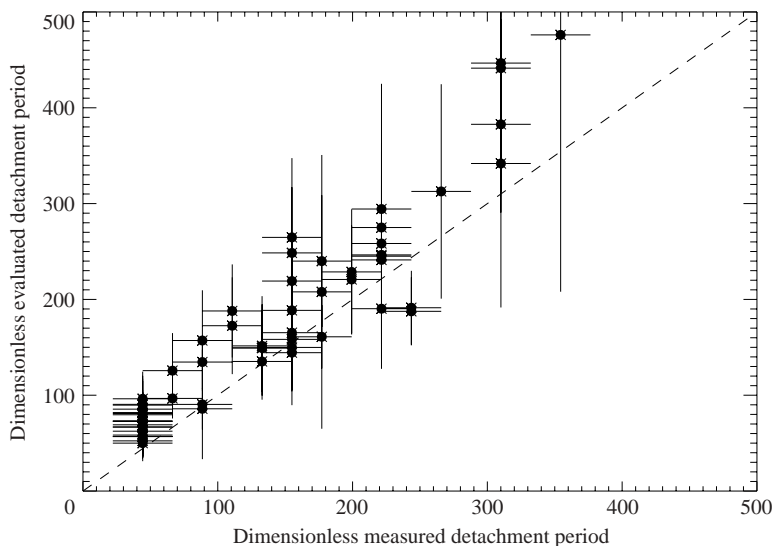


FIGURE 6. Comparison of the dimensionless detachment period predicted by (2.3) and (3.4) with that measured from the numerical experiments of §3. Detachment periods have been made dimensionless with the timescale  $\sqrt{h_c/g}$ .

$T_d^m/(\sqrt{h_c/g})$  reported along the abscissa. In fact most of the solid circles lie above the dashed line which represents perfect agreement. Error bars have been superposed which correspond to the sampling time for  $T_d^m$  and the confidence range of 95% for  $T_d^e$ .

The discrepancy between  $T_d^e$  and  $T_d^m$  can, alternatively, be measured by the relative error

$$\Delta T_d = \frac{\sum_{i=1}^N |T_{d_i}^m - T_{d_i}^e|}{\sum_{i=1}^N T_{d_i}^m} \quad (3.5)$$

which is found to be of about 28%.

Note that a natural lower limit of one detachment period per wave is seen for conditions of large waves and/or small vortices.

We believe that, notwithstanding the number of estimated parameters (like  $E_D$  and  $R$ ) influencing (2.3), such an equation provides a quite accurate and useful means for predicting  $T_d$ .

#### 4. Conclusions

Analytical examination of breaking-wave-generated macrovortices has shown a range of possible behaviours, which are mainly dependent on geometry. Startup conditions have been divided into different stages, with different processes dominant in each stage. Of these, initial acceleration of the background flow, self-advection by sloping beds, and mutual advection by oppositely signed vortices are the most important between breakwaters. The greater the tendency for deviations from the idealized conditions presented here, and very quick temporal changes in the flow regime make definitive predictions highly approximate for complex cases. Representation of the momentum-conserving processes using breaking pseudo-forces shows commonalities between considerably different phase-resolving and

phase-averaged representations: circulation is generated by the line integral of breaking pseudo-forces, with deeper water corrections in some cases.

Predictive estimates have been given for the rate of change of circulation for waves breaking on a bar or breakwater next to a deeper gap, and for the initial acceleration and detachment of macrovortices at startup. Excellent agreement has been found between predicted and computed initial detachment periods for macrovortices on isolated breakwaters. Analysis of the flow patterns and of the macrovortex trajectories allows us to clarify the fundamental role played by the beach slope in determining the features of the vortex propagation. For the case here with widely separated breakwaters, self-advection controls the dynamics. For closely spaced breakwaters or rip currents, the dynamics are very different. Here, vortex couples travel offshore instead of shoreward, and mutual interaction effects may become significant as the vortices travel into deeper water. This flow has been investigated in detail as reported in Part 2.

M. B. was supported by the European Commission Research Grant EVK3-2000-22038 (DELOS) and by the Italian MIUR. Grant “Influenza di vorticità e turbolenza nelle interazioni dei corpi idrici con gli elementi al contorno e ripercussioni sulle progettazioni idrauliche”. A. B. K. was supported by the University of Florida. L. S. and A. M. were supported by the Italian MIUR. Grant “Idrodinamica e morfodinamica di spiagge protette da opere trascinabili”.

#### REFERENCES

- BROCCHINI, M., BERNETTI, R., MANCINELLI, A. & ALBERTINI, G. 2001 An efficient solver for nearshore flows based on the WAF method. *Coastal Engng* **43**, 105–129.
- BROCCHINI, M., DRAGO, M. & IOVENITTI, L. 1992 The modelling of short waves in shallow waters. Comparison of numerical models based on Boussinesq and Serre equations. *Proc. 23th Intl Conf. Coast. Engng, ASCE*, vol. 1, pp. 76–88.
- BROCCHINI, M., MANCINELLI, A., SOLDINI, L. & BERNETTI, R. 2002 Structure-generated macrovortices and their evolution in very shallow depths. *Proc. 28th Intl Conf. Coast. Engng, ASCE*, vol. 1, pp. 772–783.
- BÜHLER, O. 2000 On the vorticity transport due to dissipating or breaking waves in shallow-water flow. *J. Fluid Mech.* **407**, 235–263.
- BÜHLER, O. & JACOBSON, T. E. 2001 Wave-driven currents and vortex dynamics on barred beaches. *J. Fluid Mech.* **449**, 313–339.
- CENTURIONI, L. R. 2002 Dynamics of vortices on a uniformly shelving beach. *J. Fluid Mech.* **472**, 211–228.
- CHEN, Q., KIRBY, J. T., DALRYMPLE, R. A., KENNEDY, A. B. & HALLER, M. C. 1999 Boussinesq modelling of a rip current system. *J. Geophys. Res.* **104**, 20617–20637.
- DEAN, R. G. & DALRYMPLE, R. A. 1984 *Water Wave Mechanics for Engineers and Scientists*. Prentice-Hall.
- DINGEMANS, M. W., RADDER, A. C. & DE VRIEND, H. J. 1987 Computation of the driving forces of wave-induced currents. *Coastal Engng* **11**, 539–563.
- GOBBI, M. F., KIRBY, J. T. & KENNEDY, A. B. 2000 On the consistency of Boussinesq models and their ability to predict vertical vorticity fields. *Proc. Intl Conf Coastal Engng, ASCE*, vol. 2, pp. 1321–1334.
- KENNEDY, A. B. 2003 A circulation description of a rip current neck. *J. Fluid Mech.* **497**, 225–234.
- KENNEDY, A. B., BROCCHINI, M., SOLDINI, L. & THOMAS, D. 2004 Topographically-controlled, breaking wave-induced macrovortices. Part 2. Rip current topographies. *J. Fluid Mech.* (submitted).
- KENNEDY, A. B., CHEN, Q., KIRBY, J. T. & DALRYMPLE, R. A. 2000 Boussinesq modeling of wave transformation, breaking and runup. I: 1D. *J. Waterway, Port Coast. Ocean Engng ASCE* **126**, 39–47.

- KENNEDY, A. B. & THOMAS, D. A. 2004 Drifter measurements in a laboratory rip current. *J. Geophys. Res.*, (submitted).
- LLOYD, P. M. & STANSBY, P. K. 1997 Shallow-water flow around model conical island of small side slope. Part I: surface piercing. *J. Hydraul. Engng ASCE* **123**, 1057–1067.
- LLOYD, P. M., STANSBY, P. K. & CHEN, D. 2001 Wake formation around islands in oscillatory laminar shallow-water flows. Part 1. Experimental investigation. *J. Fluid Mech.* **429**, 217–238.
- LONGUET-HIGGINS, M. S. 1973 The mechanics of the surf zone. *Proc. 13th Intl Congr. Theor. Appl. Mech.* **1**, 213.
- MEI, C. C. 1983 *The Applied Dynamics of Surface Ocean Waves*. John Wiley & Sons.
- PEREGRINE, D. H. 1998 Surf zone currents. *Theor. Comput. Fluid Dyn.* **10**, 295–309.
- PEREGRINE, D. H. 1999 Large-scale vorticity generation by breakers in shallow and deep water. *Eur. J. Mech. B/Fluids* **18**, 403–408.
- PRATT, L. J. 1983 On inertial flow over topography. Part 1. Semigeostrophic adjustment to an obstacle. *J. Fluid Mech.* **131**, 195–218.
- SCHÄFFER, H. A., MADSEN, P. A. & DEIGAARD, R. 1993 A Boussinesq model for waves breaking in shallow water. *Coastal Engng* **20**, 185–202.
- SCHÄR, C. & DURRAN, D. R. 1997 Vortex formation and vortex shedding in continuously stratified flows past isolated topography. *J. Atmos. Sci.* **54**, 534–554.
- SCHÄR, C. & SMITH, R. B. 1993*a* Shallow-water flow past isolated topography. Part I. Vorticity production and wake formation. *J. Atmos. Sci.* **50**, 1373–1400.
- SCHÄR, C. & SMITH, R. B. 1993*b* Shallow-water flow past isolated topography. Part II. Transition to vortex shedding. *J. Atmos. Sci.* **50**, 1401–1412.
- SMITH, J. A. & LARGIER, J. L. 1995 Observations of nearshore circulation: rip currents. *J. Geophys. Res.* **100**, 10967–10975.
- TORO, E. F. 2001 *Shock-capturing Methods for Free-surface Shallow Flows*. J. Wiley and Sons.
- VEERAMONY, J. & SVENDSEN, I. A. 2000 The flow in surf-zone waves. *Coastal Engng* **39**, 93–122.
- YU, J. & SLINN, D. N. 2003 Effects of wave-current interaction on rip currents. *J. Geophys. Res.* **108**, doi:10.129/2001JC001105.